INORGANIC CHEMISTRY

FRONTIERS

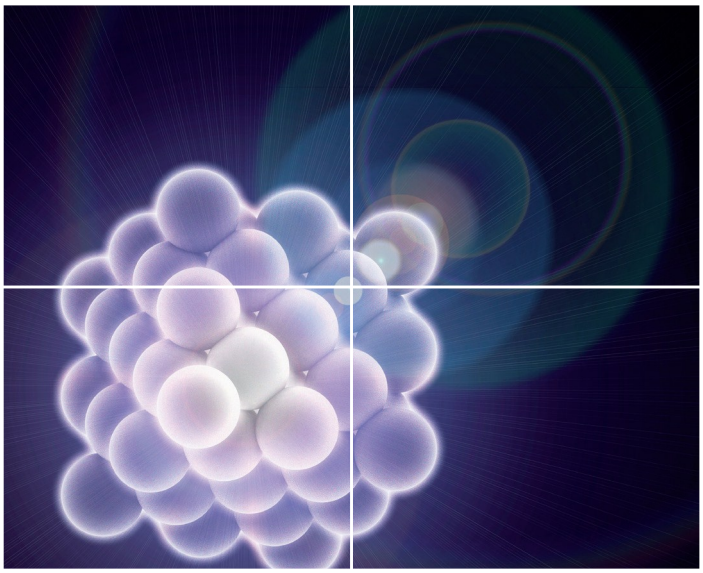

Accepted Manuscript

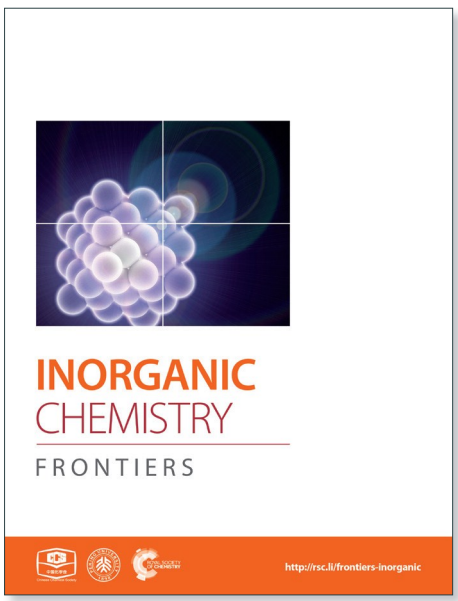

This is an *Accepted Manuscript*, which has been through the Royal Society of Chemistry peer review process and has been accepted for publication.

Accepted Manuscripts are published online shortly after acceptance, before technical editing, formatting and proof reading. Using this free service, authors can make their results available to the community, in citable form, before we publish the edited article. We will replace this *Accepted Manuscript* with the edited and formatted *Advance Article* as soon as it is available.

You can find more information about *Accepted Manuscripts* in the **Information for Authors**.

Please note that technical editing may introduce minor changes to the text and/or graphics, which may alter content. The journal's standard **Terms & Conditions** and the **Ethical guidelines** still apply. In no event shall the Royal Society of Chemistry be held responsible for any errors or omissions in this *Accepted Manuscript* or any consequences arising from the use of any information it contains.

Journal Name

ARTICLE

Assembled 3D Electrocatalysts for Efficient Hydrogen Evolution: WSe_2 Layers Anchored on Graphene Sheets

Received 00th January 20xx,
Accepted 00th January 20xx

DOI: 10.1039/x0xx00000x

rsc.li/frontiers-inorganic

Zhengqing Liu, Hongyang Zhao, Na Li, Yi Zhang, Xinyu Zhang and Yaping Du*

A new 3D composite electrocatalyst material is produced by growing WSe_2 thin layers vertically on 2D reduced graphene oxide nanosheets. The material holds the improved electrode/electrolyte interactions and efficient catalysis due to the rich defects, 3D hybrid configuration, and the direct integration of the WSe_2 onto the graphene sheets, which can significantly prevent the aggregation of WSe_2 and promote the material conductivity. As demonstrated, the as-harvested WSe_2/graphene hybrid exhibited excellent electrocatalytic activity in the hydrogen evolution reaction (HER), such as a low onset overpotential of 100 mV, small Tafel slope of 64 mV/decade and outstanding stability.

Introduction

Hydrogen is a promising candidate among the development of new, clean, and efficient energy carriers due to its high energy density.[1,2] Currently an attractive hydrogen production through electrolysis is going to stand out; running electricity through water to separate out the hydrogen and oxygen atoms. To make this process feasible, high-efficient and low-cost electrocatalysts need to be explored and developed. Although the platinum (Pt) has been demonstrated to be the efficient electrocatalyst for hydrogen evolution reaction (HER), the scarcity and high cost limit their practical application.[3,4] The transition metal dichalcogenides (TMDs) are being envisaged for HER use as their inexpensive costs and excellent electrochemical stability, and therefore great efforts have been dedicated to improving the HER performance of TMDs.[5-8]

As an important class of TMDs, tungsten selenide (WSe_2) with a typical layered crystal structure, where each layer of W atoms is sandwiched between two layers of hexagonally close-packed Se atoms, and the atomic layers are stacked by weak van der Waals interactions.[9] Additionally, the WSe_2 possesses a smaller band gap of ~1.6 eV and exhibits excellent electrical transport performance in the category of TMDs materials.[10,11] Both theoretical calculations and experimental results have already highlighted that the HER activity of TMDs materials arises from the active edge sites, indicating the unsaturated dichalcogenides atoms on the edges play an important role in HER catalysis.[12-15] However, the layered TMDs materials can be easily re-stacked due to the intrinsic interlayer vdW attractions, as a result of reducing the active edge sites.[16] Therefore, in order to further improve the catalytic performance, lots of efforts have been put to preserve the two dimensional (2D) TMDs nanostructures and introduce the desired defects, thus to design more active sites for promoting the HER activity. For instances, Cui's group developed layer vertically aligned 2D WSe_2 nanofilms with exposing more active edge sites.[17] He's group and Wang's group synthesized $WS_{2(1-x)}Se_{2x}$ and WSe_2 on carbon fibres, and assembled as working electrode, which all exhibited promising HER performance owing to the abundant catalytic edge sites and enhanced charge transfer efficiency.[18,19]

In the present study, for the first time, we established a facile one-step colloidal synthesis method to fabricate three dimensional (3D) WSe_2/rGO hybrid. This hybrid electrocatalyst was formed by selective growth of WSe_2 layers on 2D reduced graphene oxide (rGO) to obtain assembled 3D configuration (Fig. S1, ESI†). Due to the rGO as a unique support and the as-

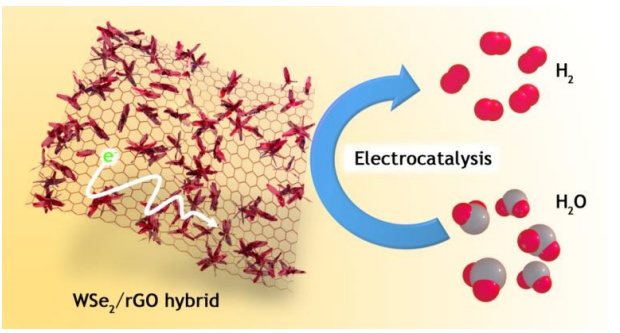

Scheme 1 Schematic illustration of 3D WSe_2/rGO hybrid assembled from layered WSe_2 anchored on graphene nanosheets and their application in HER.

Frontier Institute of Science and Technology jointly with College of Science, State Key Laboratory for Mechanical Behavior of Materials, Xi'an Jiaotong University, Xi'an 710049, China. E-mail: ypdu2013@mail.xjtu.edu.cn

Electronic Supplementary Information (ESI) available: SEM and TEM images of GO and optimal conditional experiments, the comparison of HER performance for different ratio of WSe_2/rGO hybrid catalysts. See DOI: 10.1039/x0xx00000x

resultant 3D architecture, it can significantly prevent the aggregation of WSe_2 layers and thus facilitating electron transfer as well as exposing more catalytic edge sites. As a proof of concept application, the performance of WSe_2/rGO hybrid for HER was evaluated (Scheme 1), which exhibited superior HER activity with a low onset overpotential of 100 mV and small Tafel slope of 64 mV/decade. Importantly, the HER activity of WSe_2/rGO hybrid can be maintained at least 48 h without degradation under rigid acidic conditions.

Experimental section

Chemicals

Ammonium tungstate, ($(NH_4)_2WO_4$, 99.9%) and Selenium powder (Se, 99.5%) were purchased from Alfa Aesar. Oleylamine, (OM, 70%), Oleic acid (OA, 90%), 1-dodecanethiol (1-DDT, 98%) and 15% Pt on Charcoal (Pt/C) were purchased from Sigma-Aldrich. Ethanol (AR), cyclohexane (AR) (Sinopharm Chemical Reagent Company). All chemicals were used as received without further purification. The nanocrystals were synthesized by using standard air-free procedures.

Synthesis of WSe_2 layers

A typical procedure is described as follows: First, a given amount of 0.2 mmol $(NH_4)_2WO_4$ and 16 mmol oleylamine (OM) in a three necked flask (100 mL) was heated to 120 °C to remove water and oxygen. This solution was marked as **solution A**. 4 mmol OM, 10 μL 1-dodecanethiol (1-DDT) and 0.6 mmol Se powder were deposited in a separate flask, bubbled with nitrogen (N_2) three times, and then ultrasound under N_2 atmosphere for dissolving Se powder. This solution was labeled as **solution B**. Once the Se powder was dissolved, the solution B was injected into **solution A** under vigorous stirring. After injection, the resulted mixture was heated to 280 °C under N_2 and kept at that temperature for 60 min. Upon cooling to room temperature, the products were precipitated by adding an excess of ethanol and separated from the solution by centrifugation (9500 rpm, 10 min), followed by drying in an oven at 60 °C. To remove the organic residue and excess selenium powder, the as-prepared products were annealed in Ar/H_2 (95%:5%) at 500 °C for 1 h.

Growth of WSe_2 layers on graphene

GO was made by a modified Hummers method.[20] Then functionalization of GO: 5 ml of OM and 10 ml of toluene was added to 20 mg of oven-dried GO. Subsequently, the mixture was sonicated for 30 minutes until GO was homogeneously dispersed in the solution, and then the dispersion was centrifuged at 9000 rpm for 10 minutes to collect the sediment. The sediment, referred to as OM–GO, was re-dispersed in 5 mmol of OM and kept as stock solution. The following steps were similar to the preparation of WSe_2 except adding above prepared 5 mmol of OM–GO stock solution. For comparison, the other two WSe_2/rGO hybrid nanostructures with different graphene and WSe_2 ratios were prepared: one is with 0.2 mmol of $(NH_4)_2WO_4$, 0.6 mmol of Se and 10 mg of GO; and another is with 0.2 mmol of $(NH_4)_2WO_4$, 0.6 mmol of Se and 30 mg of GO.

Characterizations

TEM images were acquired by a Hitachi HT−7700 transmission electron microscope (TEM, Japan) operating at 100 kV. High−resolution TEM (HRTEM) micrographs were obtained with a Philips Tecnai F20 FEG−TEM (The USA) operated at 200 kV. Samples for TEM analysis were prepared by drying a drop of cyclohexane solution containing the nanomaterials on the surface of a carbon−coated copper grid. Raman spectrum of powder samples were recorded on LabRAM HR Raman microscope with a laser excitation wavelength of 532 nm. The X ray diffraction (XRD) patterns were obtained using a Rigaku D/MAX−RB with monochromatized Cu Kα radiation (λ=1.5418 Å) in the 2θ ranging from 10° to 80°. X ray photoelectron spectra (XPS) were conducted using a PHI Quantera SXM instrument equipped with an Al X−ray excitation source (1486.6 eV). Binding energies (BEs) are referenced to the C 1s of carbon contaminants at 284.6 eV. All samples were prepared by depositing a thin layer of products onto a cleaned Si wafer and drying at room temperature.

Electrocatalytic measurements for HER

Typically, 4 mg of sample and 30 μL Nafion solution (5 wt%) were dispersed in 1 mL water–ethanol solution with volume ratio of 1:1 by sonicating for 1 h to form a homogeneous ink. Then 5 μL of the dispersion (containing 20 μg of catalyst) was loaded onto a rotating disk electrode (RDE) with 3 mm diameter (loading ca. 0.285 mg cm^{-2}). Linear sweep voltammetry with scan rate of 2 mV s^{-1} was conducted in 0.5 M H_2SO_4 (purged with pure N_2) using electrochemical cell setup, with a saturated calomel electrode ($Hg/HgCl_2$ in saturated KCl) as the reference electrode and a Pt plate as the counter electrode, and RDE as the working electrode with a rotating speed of 1600 rpm. All the potentials were converted to values with reference to a reversible hydrogen electrode (RHE). Cyclic voltammetry was conducted at room temperature by using the same standard three-electrode setup ranging from 0.3 to 0.4 V (vs. RHE) at a scan rate of 20, 40, 60, *et.al.* mV s^{-1}. Time-dependent current density curve of WSe_2 and WSe_2/rGO hybrid was conducted under static overpotential of -700 mV (vs. SCE) for continuous operation of 48 h. Nyquist plots of WSe_2 layers and WSe_2/rGO hybrid were measured on the AUTOLAB PGSTAT204 electrochemistry workstation in the frequency range from 0.1 Hz to 100 kHz at an open circuit potential with 10 mV as the amplitude potential. WSe_2/rGO hybrid and pure WSe_2-coated CFPs (1 cm^2, catalyst loading 1 mg) were used as working electrodes to collect chronoamperometry data at the applied potential of -0.7 V vs. SCE.

Results and discussions

Fig. 1a shows the X-ray diffraction (XRD) patterns of WSe_2 layers and WSe_2/rGO hybrid. All of diffraction peaks corresponding to the typical hexagonal WSe_2 (space group: P63/mmc, $a = b = 0.329$ nm, $c = 1.298$ nm, JCPDS: 38−1388) are detected in WSe_2/rGO hybrid, and no diffraction peaks from any other chemical species are detectable in both WSe_2 layers and WSe_2/rGO hybrid samples. The nealry similar XRD patterns for WSe_2 layers and WSe_2/rGO hybrid shown in Fig. 1a may be owing to the high crystallizaion of WSe_2, as a result of the rGO's XRD signals are too weak to observe. The transmission electron microscopy (TEM) and scanning electron microscope (SEM) images shown in Fig. 1b and S2a demonstrate the formation of WSe_2 with 2D layered structures. As seen from the SEM and TEM images shown in Fig. 1c and d, the rGO nanosheets are decorated with uniform WSe_2 layers and no free WSe_2 left in the solution (Fig. S2b, ESI†), indicating the graphene nanosheets afford a good platform for the nucleation and subsequent growth of WSe_2 layers. The mechanism responsible for WSe_2 layers selective grown on rGO is possible due to the precursors are anchored to GO through functional groups (*e.g.* carboxyl, hydroxyl, and epoxy), and the defects on the graphene would act as the nucleation sites.[12,21-23] Notably, the vertical WSe_2 layers could be clearly visible in the enlarged SEM image (inset of Fig. 1c) of WSe_2/rGO hybrid. Such nanostructured material can offer a much rougher surface, reduce the solid–gas interaction and thereby enhancing the HER performance.[24,25] The energy dispersive X-ray spectroscopy (EDS) data (Fig. S2c, ESI†) verifies the stoichiometric atomic ratio for W:Se in the as-formed WSe_2 (W: Se = 1:2).

The high-resolution TEM (HRTEM) images taken from different positions of WSe_2 layers grown on rGO show clear lattice fringes, demonstrating the as-obtained WSe_2 layers is of high crystallinization (Fig. 2a and b). As seen from the planar orientation (Fig. 2a), WSe_2 shows lattice fringes with interplane spacing of ~0.28 nm and the fast Fourier transformation (FFT) pattern (inset of Fig. 2a) exhibits six independent diffraction arcs, which can be both indexed to the (100) plane of hexagonal (2H-type) WSe_2. Moreover, the present diffraction arcs of FFT pattern can be attributed to the quasiperiodic structure with rich defects.[26] Meanwhile, the layered structure with interlayer spacing of ~0.64 nm and ~0.28 nm can be observed from the vertically stacked WSe_2 layers (Fig. 2b), corresponding to the (002) and (100) plane of the WSe_2, respectively, meanwhile, the FFT pattern (inset of Fig. 2b) reveals the orientation of layers along the <001> direction. Importantly, the HRTEM images also demonstrate that there are lots of defects (highlighted in circular area of Fig. 2a and b) in the present WSe_2 layers, which are expected to serve as active sites to improve the HER catalytic performance.[26,27-29] The corresponding crystal structure model shown in Fig. 2c-e can foster understanding of the as-harvested WSe_2 structure illustrated from the HRTEM images. Viewed from the <001> direction (Fig. 2d), the WSe_2 hold the graphene-like structure and (100) plane is labeled out, which is consistent with the HRTEM image shown in Fig. 2a. Moreover, viewed from the <010> direction (Fig. 2e), just like the vertically standing WSe_2 layers, the (100) and (002) planes are marked out respectively, also is corresponding well to the HRTEM image showin in Fig. 2b.

The detailed structure and chemical state for WSe_2/rGO hybrid were investigated by Raman spectroscopy and X-ray photoelectron spectroscopy (XPS). Fig. 3a shows the Raman spectrum of WSe_2/rGO hybrid, due to the small energy difference between A_{1g} (out-of-plane) (253 cm^{-1}) and E^1_{2g} (inplane) mode (250 cm^{-1}), there is only one broad peak seated from 200 to 400 cm^{-1}.[30] Meanwhile, the characteristics of graphene Raman shift for D, G, and 2D bands can be observed in WSe_2/rGO hybrid (Fig. 3a).[31] The XPS spectum of W is shown in Fig. 3b, and the binding energies of W $4f_{7/2}$ and

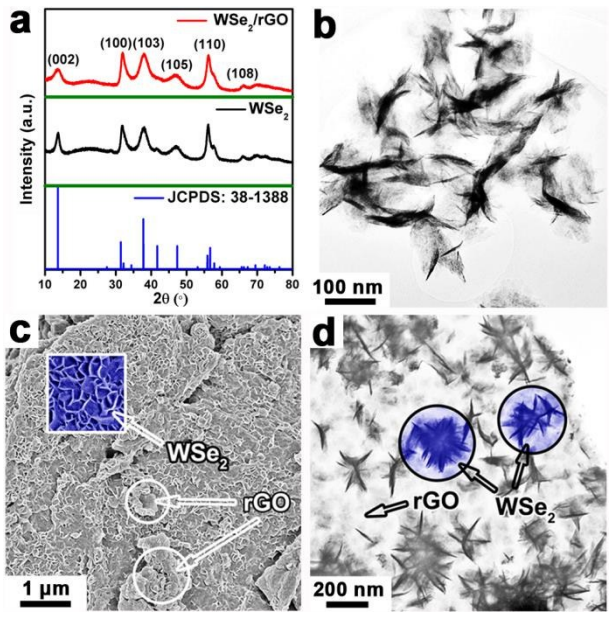

Fig. 1 (a) XRD patterns, TEM image of (b) WSe_2 layers, (c) SEM and (d) TEM images of WSe_2/rGO hybrid. Insets of square area (c) the enlarged SEM image and circular area (d) TEM image of WSe_2 grown on rGO sheets.

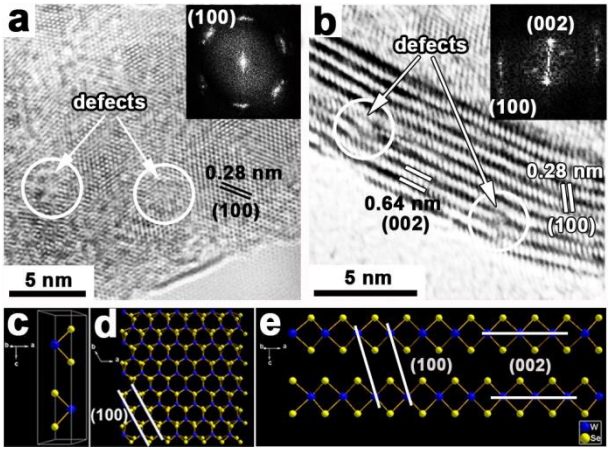

Fig. 2 HRTEM images of (a) planar and (b) vertically stacked WSe_2 layers grown on rGO. Inset of (a) and (b) are the corresponding FFT patterns. (c) The unit cell of hexagonal WSe_2 with its atom layer from <001> direction Se-[Se-W-Se-Se-W-Se]-Se. The modeling structure of WSe_2 viewed from the (d) <001> and (e) <010> direction, respectively.

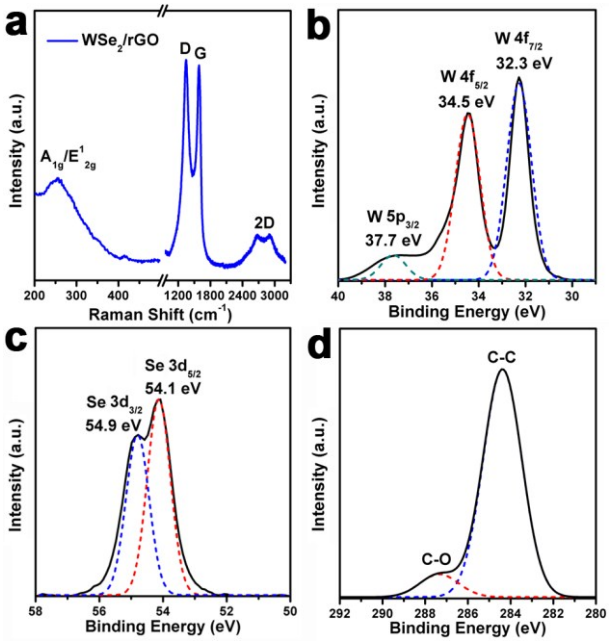

Fig. 3 Raman and XPS spectra of WSe_2/rGO hybrid. (a) A_{1g} and E^1_{2g} Raman modes of WSe_2/rGO hybrid, and D, G, and 2D bands for rGO nanosheets. (b-d) XPS spectra of W 4f, Se 3d and C 1s signals recorded for WSe_2/rGO hybrid.

W $4f_{5/2}$ locate at 32.3 and 34.5 eV indicated that the element chemical state of W are mainly quadrivalent for the WSe_2/rGO hybrid.[32] Meanwhile, the small peak located at 37.7 eV is ascribed to the core levels of W $5p_{3/2}$ from WO_3 due to the partial oxidation of WSe_2 layers.[17] Two intense peaks at 54.1 and 54.9 eV (Fig. 3c) attributable to the core levels of Se $3d_{5/2}$ and Se $3d_{3/2}$, respectively, are the characteristic of Se^{2-} of WSe_2/rGO hybrid.[33,34] The C 1s XPS signal shown in Fig. 3d demonstrated there was trace amount of oxygen content in WSe_2/rGO hybrid, confirming the reduction of GO to rGO.[35]

In present synthesis, the combination of capping ligands (OA and OM) and the amount of Se powder precursor were found to play crucial roles in the formation of high-quality WSe_2 products. For example, fixing the amount of solvent (20 mmol) and the mole ratio of $(NH_4)_2WO_4$ and Se powder ($(NH_4)_2WO_4$: Se = 1:3), when using 0.2 mmol of $(NH_4)_2WO_4$, 0.6 mmol of Se and pure OM as solvent at 280 °C for 60 min, the pure phase WSe_2 products were obtained (Fig. 1a). Under the same reaction condition, except using OA as solvent (*e.g.* OM:OA=1:1 and pure OA), the harvested products possessed layered structure (Fig. S3a and b, ESI†), but coexisted with a small amount of tungsten oxide (WO_3) (Fig. S3c, ESI†). In addition, when the mole ratio of $(NH_4)_2WO_4$ and Se powder larger than 1:3 (*e.g.*1:2, 0.2 mmol of $(NH_4)_2WO_4$, 0.4 mmol Se) in pure OM at 280 °C for 60 min, the as-prepared samples also contained considerable impurities with nanorods morphology (Fig. S4a and b, ESI†). To conclude, after series of condition based experiments, we found that high-quality WSe_2 layers can be obtained in 20 mmol of OM solvent at temperature of 280 °C for 60 min under precursor concentration of 0.2 mmol $(NH_4)_2WO_4$ and 0.6 mmol Se powder, which can elegantly maintain the balance between nucleation and growth stages (Fig. 1b and Fig. S2a, ESI†).

The HER electrocatalytic performance of as-prepared WSe_2 layers and WSe_2/rGO hybrid were investigated by using a standard three-electrode setup with the same loading value of 0.285 mg cm^{-2} on a rotating disk electrode (RDE) in 0.5 M H_2SO_4 electrolyte degassed with N_2 (Experimental section,). As shown in Fig. 4a, the polarization curves (iR corrected) showed the current density versus voltage (J versus V) for the comparison of WSe_2 layers and WSe_2/rGO hybrid along with Pt/C (15%) samples. As depicted from Fig. 4a, only rGO had no HER activity, hinting that the core catalysts were WSe_2 layers. Compared with pure WSe_2 layers, the onset potential of WSe_2/rGO hybrid shifted from -160 mV to -100 mV and significant H_2 evolution (J = 10 mA cm^2) was observed at −180 mV, which was much smaller than WSe_2 (−307 mV) vs. RHE, suggesting the excellent catalytic activity of the WSe_2/rGO hybrid. In order to further study the HER electrocatalytic performance of WSe_2/rGO hybrid, WSe_2 layers physically mixed with rGO (WSe_2+rGO) having the same ratio of WSe_2/rGO hybrid was also performed, which exhibited much lower HER catalytic activity (Fig. S5a, ESI†). The superior HER catalytic performance of WSe_2/rGO hybrid compared to WSe_2+rGO may be due to the improved charge transfer efficiency between the WSe_2 layers and rGO.[12,36] In addition, HER electrocatalytic activities of WSe_2/rGO hybrids with different WSe_2 to rGO content ratios were measured.(Fig. S5b, ESI†). When the loading density of WSe_2 on rGO is higher (0.2 mmol WSe_2/10 mg rGO), a relative lower catalytic performance is obtained, probably due to the lower efficiency of charge transfer.[26,37] On the contrary, when the loading density of WSe_2 on rGO is lower (0.2 mmol WSe_2/30 mg rGO), the inferior catalytic performance is resulted from the less loading density of core catalysts of WSe_2. Thus, the 0.2 mmol of WSe_2 loaded on 20 mg of graphene (0.2 mmol WSe_2/20 mg rGO) is the optimized content ratio for fulfilling the best HER performance.

The promising enhancement in HER activity (Fig. 4b) was apparent by comparing the Tafel slopes of WSe_2/rGO hybrid (64 mV/decade, after iR correction) with pure WSe_2 layers (126 mV/decade, after iR correction), demonstrating the kinetic speed of electrochemical hydrogen evolution for WSe_2/rGO hybrid was much faster than the pure WSe_2 layers. This Tafel slope was also comparable to or even lower than the previous reported WSe_2-based HER catalysts (Table S1). Generally, Tafel slope includes three principal steps in converting H^+ to H_2 in HER:[12,38-40]

$$H_3O^+ + e - M \leftrightarrow H - M + H_2O$$ (Volmer reaction) (1)

$$2H - M \leftrightarrow H_2 - M + M$$ (Tafel reaction) (2)

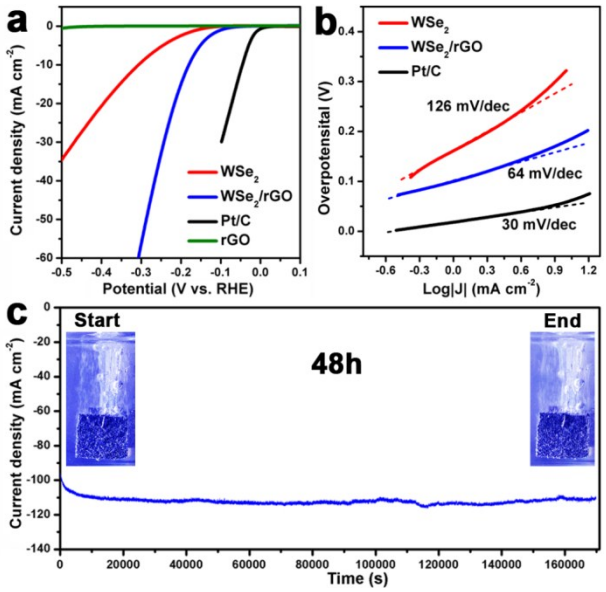

Fig. 4 (a) Polarization curves of WSe_2 layers, WSe_2/rGO hybrid, rGO and Pt/C (15%). (b) The corresponding Tafel curves and (c) durability test by continuous HER recorded on WSe_2/rGO hybrid-modified CFP electrode at a static overpotential of -0.7 V vs. SCE. The catalysts were deposited on CFP with loading concentration of 1 mg cm^{-2}. Inset of (c): digital photos showing the H_2 bubbles formed on WSe_2/rGO hybrid-modified CFP at the time point of start and end (48 h). All the measurements were performed in N_2 saturated 0.5 M H_2SO_4 electrolyte.

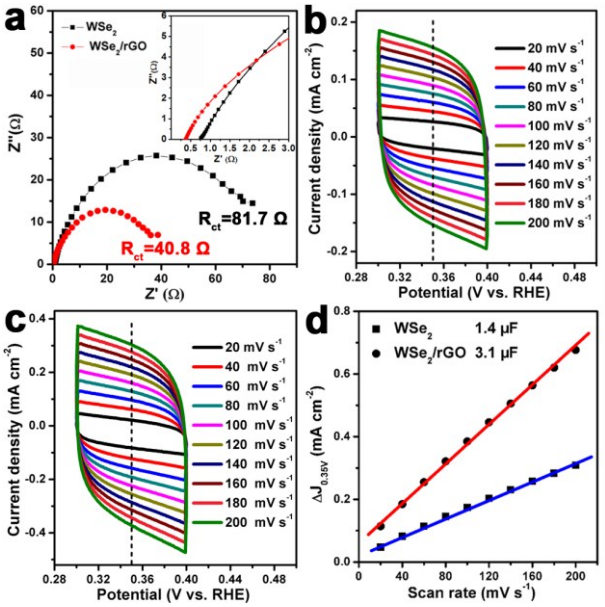

Fig. 5 (a) EIS Nyquist plots. Voltammograms of the (b) WSe_2 layers and (c) WSe_2/rGO hybrid electrocatalysts at various scan rates (20–200 mV s^{-1}). (d) Estimated C_{dl} and relative electrochemically active surface area for WSe_2 layers and WSe_2/rGO hybrid electrocatalysts. The inset of (a) shows the high frequency Nyquist plots of the two catalysts.

$$H_3O^+ + e - M + H - M \leftrightarrow H_2 - M + M + H_2O \quad \text{(Heyrovsky reaction)} \quad (3)$$

Where, e−M represents catalyst-bound electrons and H−M and H_2−M stand for hydrogen atom and molecule adsorbed onto catalyst surface, respectively. The first step (1) is a discharge step (Volmer reaction, 120 mV/dec), in which protons (H_3O^+) are adsorbed to active sites on the catalysts surface and combined with electrons (e−M) to form adsorbed hydrogen atoms (H−M). The following process is the combination step (2) (Tafel reaction, 30 mV/dec) or desorption step (3) (Heyrovsky reaction, 40 mV/dec). In present work, Tafel slope is 64 mV/decade for the WSe_2/rGO hybrid (Fig. 4b), indicating the Heyrovsky reaction plays a crucial role in determining HER rate of WSe_2/rGO hybrid.

Apart from current density and Tafel slope, the stability of catalyst is another important criterion for HER. The long-term stability of WSe_2 layers and WSe_2/rGO hybrid catalysts is conducted by means of continuous HER at static overpotential of -0.7 V vs. SCE in 0.5 M H_2SO_4 for 48 h. The WSe_2 layers and WSe_2/rGO hybrid catalysts are loaded on carbon fibre paper (CFP) with a high catalyst loading concentration of 1 mg cm^{-2} (Experimental section). As shown in Fig. 4c, the current density of WSe_2/rGO hybrid modified CFP electrode increase gradually at the initial ~2 h and then stable even after a long period of 48 h. Furthermore, digital photos (inset of Fig. 4c) taken from WSe_2/rGO hybrid modified CFP electrode at the start and end of durability test, show the vigorous effervescence of H_2 bubbles (Movie 1, ESI†). Remarkably, the XPS spectra of WSe_2/rGO hybrid after the HER for 48 h show no obvious change about the chemcial state of both Mo and Se elements (Fig. S6a and b, ESI†), indicating the WSe_2/rGO hybrid catalyst are rather stable in an rigid acidic environment for a long time. By comparison, under the same HER condition, the pure WSe_2 exhibited a relative fluctuation in HER activity after 11 h (Fig. S7, ESI†).

The smaller (64 mV/decade) Tafel slope, lower onset potential (-100 mV) and outstanding stability verify the WSe_2/rGO hybrid can be an effective electrocatalyst for HER. We also performed the electrochemical impedance spectroscopy (EIS) of WSe_2 layers and WSe_2/rGO hybrid to investigate the electrode kinetics for HER. The Nyquist plots of WSe_2 layers and WSe_2/rGO hybrid samples are compared (Fig. 5a) and fitted to an equivalent circuit (Fig. S8, ESI†), where a constant phase element (CPE) is employed. As displayed in Fig. 5a, Nyquist plots reveal a decrease in charge-transfer resistance (R_{ct}) for WSe_2/rGO hybrid (40.8 Ω) as compared to the pure WSe_2 layers (81.7 Ω), indicating a smaller reaction resistance and higher catalytic activity for HER in acid solution for WSe_2/rGO hybrid electrode. In addition, as shown in the inset of Fig. 5a, the WSe_2/rGO hybrid also exhibited a smaller Rs (0.4 Ω) than WSe_2 layers (0.8 Ω), demonstrating that our one-pot synthesis strategy for growth of WSe_2 layers on graphene could also improve the electrical contact at the interface of the electrode.

We further compared the electrochemical surface area (ECSA) of WSe_2 layers and WSe_2/rGO hybrid samples by measuring the double-layer capacitance (C_{dl}). Fig. 5b and c show the typical cyclic voltammograms (CVs) of WSe_2 layers and WSe_2/rGO hybrid taken with various scan rates (20-200 mV/s^{-1}) in the region of 0.3-0.4 V (vs. RHE) in 0.5 M H_2SO_4, respectively. Current density differences ($\Delta J = J_a - J_c$) at 0.35 V

(vs. RHE) are then plotted against scan rate. The electrochemical double-layer capacitances, which are equivalent to half of the linear slopes in Fig. 5d, are used to represent and compare the ECSA of WSe_2 layers and WSe_2/rGO hybrid. It is noteworthy that the C_{dl} of WSe_2/rGO hybrid (3.1 μF) is much higher than that of WSe_2 layers (1.4 μF), suggesting that WSe_2/rGO hybrid possesses much larger active surface area and more active sites for hydrogen production.[8,41]

Three possible reasons could be responsible for the excellent HER performance of 3D WSe_2/rGO hybrid nanostructures. Firstly, since the WSe_2 layers are vertically grown on the rGO, which can effectively reduce the agglomeration of WSe_2 layers, maximally expose the active edges and reduce the solid–gas interaction. Secondly, the charge transfer efficiency at the electrode interface is greatly promoted through combining the high electrical conductive rGO. The last one is that the defects-rich structure of WSe_2/rGO hybrid, which is contributed to the additional clatlytic active sites.

Conclusions

In summary, the WSe_2/rGO hybrid nanostructures has been constructed through a facile colloidal chemistry method and developed as a HER catalyst electrode, which exhibits excellent HER activity with a low onset potential of 100 mV, small Tafel slope of 64 mV/decade and excellent stability. The Tafel slope of 64 mV/dec suggests a Volmer–Heyrovsky mechanism for the catalyzed HER. These findings can be attributed to the uniform distribution of WSe_2 layers on the rGO, rGO high electrical conductivity and rich defects in the hybrid structrues. The work presented in this paper will spur the research on improving the activity of TMDs-based electrocatalysts for HER.

Acknowledgements

We gratefully acknowledge the financial aid from the start-up funding from Xi'an Jiaotong University, the Fundamental Research Funds for the Central Universities (2015qngz12), the NSFC (grant no. 21371140), and the China National Funds for Excellent Young Scientists (grant no. 21522106).

Notes and references

1 J. A. Turner, *Science*, 2004, **305**, 972.
2 B. Winther-Jensen, K. Fraser, C. Ong, M. Forsyth and D. R. MacFarlane, *Adv. Mater.*, 2010, **22**, 1727.
3 E. Antolini, *Energy Environ. Sci.*, 2009, **2**, 915.
4 C. L. Tan and H. Zhang, *Chem. Soc. Rev.*, 2015, **44**, 2713.
5 D. Voiry, H. Yamaguchi, J. W. Li, R. Silva, D. C. B. Alves, T. Fujita, M. W. Chen, T. Asefa, V. B. Shenoy, G. Eda and M. Chhowalla, *Nat. Mater.*, 2013, **12**, 850.
6 J. Kibsgaard, Z. B. Chen, B. N. Reinecke and T. F. Jaramillo, *Nat. Mater.*, 2012, **11**, 963.
7 L. Cheng, W. J. Huang, Q. F. Gong, C. H. Liu, Z. Liu, Y. G. Li and H. J. Dai, *Angew. Chem., Int. Ed.*, 2014, **53**, 7860.
8 M. A. Lukowski, A. S. Daniel, F. Meng, A. Forticaux, L. S. Li and S. Jin, *J. Am. Chem. Soc.*, 2013, **135**, 10274.
9 W. Zhao, Z. Ghorannevis, L. Chu, M. Toh, C. Kloc, P. H. Tan and G. Eda, *ACS Nano*, 2012, **7**, 791.
10 Q. H. Wang, K. Kalantar-Zadeh, A. Kis, J. N. Coleman and M. S. Strano, *Nat. Nanotechnol.*, 2012, **7**, 699.
11 H. J. Chuang, X. B. Tan, N. J. Ghimire, M. M. Perera, B. Chamlagain, M. M. C. Cheng, J. Q. Yan, D. Mandrus, D. Tomanek and Z. X. Zhou, *Nano Lett.*, 2014, **14**, 3594.
12 Y. Li, H. Wang, L. Xie, Y. Liang, G. Hong and H. Dai, *J. Am. Chem. Soc.*, 2011, **133**, 7296.
13 T. Li and G. Galli, *J. Phys. Chem. C*, 2007, **11**, 16192.
14 D. Merki, S. Fierro, H. Vrubel and X. Hu, *Chem. Sci.*, 2011, **2**, 1262.
15 T. F. Jaramillo, K. P. Jørgensen, J. Bonde, J. H. Nielsen, S. Horch and I. Chorkendorff, *Science*, 2007, **317**, 100.
16 K. Chang, W. Chen, L. Ma, H. Li, H. Li, F. Huang, Z. Xu, Q. Zhang and J. Lee, *J. Mater. Chem.*, 2011, **21**, 6251.
17 H. Wang, D. Kong, P. Johanes, J. J. Cha, G. Zheng, K. Yan, N. Liu and Y. Cui, *Nano lett.*, 2013, **13**, 3426.
18 K. Xu, F. Wang, Z. Wang, X. Zhan, Q. Wang, Z. Cheng, M. Safdar and J. He, *ACS nano*, 2014, **8**, 8468.
19 M. Zou, J. Zhang, H. Zhu, M. Du, Q. Wang, M. Zhang and X. Zhang, *J. Mater. Chem. A*, 2015, **3**, 12149.
20 D. C. Marcano, D. V. Kosynkin, J. M. Berlin, A. Sinitskii, Z. Z. Sun, A. Slesarev, L. B. Alemany, W. Lu and J. M. Tour, *ACS Nano*, 2010, **4**, 4806.
21 Y. Shi, W. Zhou, A. Y. Lu, W. Fang, Y. H. Lee, A. L. Hsu, S. M. Kim, K. K. Kim, H. Y. Yang, L. J. Li, J. C. Idrobo and J. Kong, *Nano Lett.*, 2012, **12**, 2784.
22 H. Wang, J. T. Robinson, G. Diankov and H. Dai, *J. Am. Chem. Soc.*, 2010, **132**, 3270.
23 H. Wang, L. F. Cui, Y. Yang, H. S. Casalongue, J. T. Robinson, Y. Liang, Y. Cui and H. Dai, *J. Am. Chem. Soc.*, 2010, **132**, 13978.
24 Z. Y. Lu, Y. J. Li, X. D. Lei, J. F. Liu and X. M. Sun, *Mater. Horiz.*, 2015, **2**, 294.
25 Z. Y. Lu , W. Zhu , X. Y. Yu , H. C. Zhang , Y. J. Li , X. M. Sun, X. W. Wang , H. Wang , J. M. Wang , J. Luo, X. D. Lei and L. Jiang, *Adv. Mater.*, 2014, **26**, 2683.
26 J. Xie, H. Zhang, S. Li, R. Wang, X. Sun, M. Zhou, J. F. Zhou, X. W. Lou and Y. Xie, *Adv. Mater.*, 2013, **25**, 5807.
27 C. B. Roxlo, H. W. Deckman, J. Gland, S. D. Cameron and R. R. Chianelli, *Science*, 1987, **235**, 1629 .
28 W. Kautek and H. Gerischer, *Surf. Sci.*, 1982, **119**, 46.
29 R. R. Chianelli, A. F. Ruppert, S. K. Behal, B. H. Kear, A. Wold and R. Kershaw, *J. Catal.*, 1985, **92**, 56.
30 J. H. Yu, H. R. Lee, S. S. Hong, D. Kong, H. W. Lee, H. Wang, F. Xiong, S. Wang and Y. Cui, *Nano Lett.*, 2015, **15**, 1031.
31 A. C. Ferrari, J. C. Meyer, V. Scardaci, C. Casiraghi, M. Lazzeri, F. Mauri, S. Piscanec, D. Jiang, K. S. Novoselov, S. Roth and A. K. Geim, *Phys. Rev. Lett.*, 2006, **97**, 187401.
32 A. Katrib, F. Hemming, P. Wehrer, L. Hilaire and G. Maire, *J. Electron. Spectrosc. Relat. Phenom.*, 1995, **76**, 195.
33 W. A. Abdallah and A. E. Nelson, *J. Mater. Sci.*, 2005, **40**, 2679.
34 N. D. Boscher, C. J. Carmalt and I. P. Parkin, *J. Mater. Chem.*, 2006, **16**, 122.
35 D. Wan, C. Yang, T. Lin, Y. Tang, M. Zhou, Y. Zhong, F. Huang and J. Lin, *ACS Nano*, 2012, **6**, 9068.
36 Z. Liu, N. Li, H. Zhao and Y. Du, *J. Mater. Chem. A*, 2015, **3**, 19706.
37 H. Vrubel, D. Merki and X. Hu, *Energy Environ. Sci.*, 2012, **5**, 6136.
38 W. Zhou, D. Hou, Y. Sang, S. Yao, J. Zhou, G. Li, L. Li, H. Liu and S. Chen, *J. Mater. Chem. A*, 2014, **2**, 11358.
39 J. G. N. Thomas, *Trans. Faraday Soc.*, 1961, **57**, 1603.
40 W. Zhou, J. Zhou, Y. Zhou, J. Lu, K. Zhou, L. Yang, Z. Tang, L. Li and S. Chen, *Chem. Mater.*, 2015, **27**, 2026.

41 D. Kong, H. Wang, Z. Lu and Y. Cui, *J. Am. Chem. Soc.*, 2014, **136**, 4897.